Journal of Thermal Analysis and Calorimetry, Vol. 96 (2009) 2, 335–345

MICROSTRUCTURE DEVELOPMENT IN MIXES OF CALCIUM ALUMINATE CEMENT WITH SILICA FUME OR FLY ASH

Ana Hidalgo[*]*, J. L. García, M*[a] *Cruz Alonso, L. Fernández and Carmen Andrade*

Instituto de Ciencias de la Construcción Eduardo Torroja (IETcc-CSIC), Químico Física de Materiales de Construcción, Madrid 28033, Spain

The most widely identified degradation process suffered by calcium aluminate cement (CAC) is the so-called conversion of hexagonal calcium aluminate hydrate to cubic form. This conversion is usually followed by an increase in porosity determined by the different densities of these hydrates and the subsequent loss of strength.

Mixes of calcium aluminate cement (CAC) and silica fume (SF) or fly ash (FA) represent an interesting alternative for the stabilization of CAC hydrates, which might be attributed to a microstructure based mainly on aluminosilicates.

This paper deals with the microstructure of cement pastes fabricated with mixtures CAC-SF and CAC-FA and its evolution over time. Thermal analysis (DTA/TG), X-ray diffraction (XRD) and mid-infrared spectroscopy (FTIR) have been used to assess the microstructure of these formulations.

Keywords: *calcium, aluminate cement, fly ash, microstructure, silica fume, TG-DTA, WAXS*

Introduction

The main difference between Portland and calcium aluminate cements lies in the nature of the active phase that leads to setting and hardening. Monocalcium aluminate (CA) is the principal active phase in the CAC cement which reacts with water to give calcium aluminate hydrates.

The hydration reaction of calcium aluminate cement (CAC) at environmental temperatures produces hexagonal hydrated calcium aluminates $CaAl_2O_{14}H_2O$ (CAH_{10}) and $Ca_2Al_2O_{13}H_{16}$ (C_2AH_8). However the stable phases are C_3AH_6 ($Ca_3Al_2(OH)_{12}$) and AH_3 ($Al(OH)_3$) and the other phases will inevitably convert to these [1–5].

Conversion reactions are shown schematically below:

$$3CAH_{10} \rightarrow C_3AH_6 + 2AH_3 + 18H \quad (1)$$

$$3C_2AH_8 \rightarrow 2C_3AH_6 + AH_3 + 9H \quad (2)$$

where CAH_{10}: $CaAl_2O_{14}H_2O$, C_2AH_8: $Ca_2Al_2O_{13}H_{16}$, C_3AH_6: $Ca_3Al_2(OH)_{12}$, AH_3: $Al(OH)_3$ and H: H_2O.

Some authors [6–9] have found that an interesting way to reduce the hydrate conversion and the decreasing of strength is to replace some of the CAC by blast furnace slag (BFS) or a pozzolan such as microsilica and metakaolin. Majumdar showed that with concrete based on equal amounts of CAC and BFS cured at either 293 or 311 K, the compressive strength increased continuously over a period of one year, in contrast to control samples made without any BFS content, which showed decreases in strength associated with conversion. These concretes have also shown good chemical resistance and reduced temperature rise on curing [10, 11].

The reaction that avoids the conversion process could be produced in the following way [5, 11–13]: the silica content of the mineral admixtures would react initially with the calcium aluminates avoiding the formation of C_2AH_8 and, subsequently the conversion in C_3AH_6. Therefore, instead this cubic phase, a hexagonal hydrate called gehlenite ($Ca_2Al_2SiO_7{\cdot}8H_2O$; C_2ASH_8) is proposed to be formed. Majumdar *et al*. [7] considered that the amount of C_2ASH_8 is dependent on the capacity of a mineral admixture to release silica.

Although studies about stabilisation of CAC with mineral admixtures are scarce, gehlenite has been observed in CAC mixes with BFS and ther pozzolanic materials, such as the metakaolin and the silica fume (SF) [6, 9, 11, 12, 14]. Although the microsilica favours the gehlenite formation [15], some authors [10] pointed out that it does not prevent the hydrogarnet formation. However, Majumdar *et al*. 1990 and Fu *et al*. [14] concluded that, in mixes based on CAC with a silica fume content between 30 and 50%, the gehlenite is the main hydration product before a week (T^a<40°C).

Some authors [16] reported that in the system CAC-SF, silica reacts with the calcium aluminate phases in the cement and water to form different

* Author for correspondence: ahidalgo@ietcc.csic.es

1388–6150/$20.00
© 2009 Akadémiai Kiadó, Budapest
Akadémiai Kiadó, Budapest, Hungary
Springer, Dordrecht, The Netherlands

crystalline hydrates (with variable proportions of Ca, Al, Si) such as $Ca_2Al_2SiO_7{\cdot}8H_2O$ (C_2ASH_8; gehlenite), $Ca_3Al_2(SiO_4)_{3-x}(OH)_{4x}$ ($0<x<3$) (katoite) and not very well defined and complex zeolite-type phases.

The reaction of CAC with fly ash (FA) has been analysed by Collepardi *et al*. [12] indicating as conclusion of the study that FA is not suitable for reducing the transformation of hexagonal hydrates into the cubic phases. Authors pointed out that it would be necessary to use a high content of FA (>40%) in order to detect some effect in the conversion process and this percentage of mineral addition in the formulation would cause an increase in the water/cement ratio, what would produce a decrease in the compressive strength.

The aim of this work was the evaluation of the microstructure development in calcium aluminate cements blended with fly ash and silica fume. Thermal analysis (DTA/TG), X-ray diffraction (XRD) and Fourier Midinfrared Spectroscopy (FTMIR) were used to characterize the microstructural evolution of the fabricated cement pastes. Those techniques are commonly used in recent works where the hydration process of mixes composed of cements plus mineral admixtures and related materials is evaluated [17–22]. Furthermore, as early as 1978, Midgley [23] used the thermal analysis methods to assess the quality of concretes based on CAC, estimating their conversion degree.

Experimental

Materials

Calcium aluminate cement supplied by Cementos Molins (Sant Vicenç dels Horts, Barcelona, Spain), silica fume supplied by Ferroatlántica, SL. (A Coruña, Spain) and fly ash supplied by Cia. Valenciana de Cementos Pórtland S.A (Alcalá de Guadaira, Sevilla, Spain), were used for the testing program. Fly ash was classified as Class F according to the ASTM definition. Chemical composition of raw materials is presented in Table 1.

Cement pastes were fabricated with a water/binder=0.5, being their formulations 100% CAC (ref), 80% CAC+20% SF (20SF), 70% CAC+30% SF (30SF), 50% CAC+50% SF (50SF), 70% CAC+30% FA (30FA) and 50% CAC+50% FA (50FA). Deionised water was used for mixes, that were hydrated in sealed conditions (98% relative humidity and 293±2 K). Hydration was stopped at 2, 7, 30 and 90 days; the cement pastes were grounded to a powder with particle size lower than 75 μm and the process of hydration was interrupted in each case by 'freezing' the sample with ethanol and acetone.

X-ray diffraction of mineral additions (not shown) indicated that the silica fume employed in this study has a very low crystallinity and it is composed mainly by quartz and cristobalite. The X-ray spectra of the fly ash indicated that it was mainly composed of mullite, quartz, magnetite, CaO, calcite and glassy phases.

Methods

DTA/TG data were obtained from a DTA/TG SEIKO 320U thermal analyzer with a resolution of 0.01 mg. The sample was taken in a platinum crucible and heated from room temperature to 1473 K at a heating rate of 10 K min^{-1} using nitrogen as a medium under static condition. Alumina powder was used as the reference material.

Cement pastes were analyzed by X-ray diffraction (XRD) from a 2θ value of 5 to 60° with a Philips PW1710 instrument using a step of 0.02° and CuK_{α_1} radiation.

Mid-infrared spectra were taken at room temperature with a Fourier transform IR spectrometer (FTMIR) equipped with a DTGS detector and a CsI beam splitter. For each sample, 256 scans were recorded in the 4000–250 cm^{-1} spectral range with a resolution of 4 cm^{-1}. Test samples were prepared by mixing cement pastes with potassium bromide in an agate mortar, fabricating the 12 mm diameter dried KBr pellets (0.15 mg of sample and 150 mg of KBr).

Results and discussion

Thermal analysis (DTA/TG)

The identification of mineral components in such complex mixtures and their quantification, using DTA/TG is difficult and often may be impossible due to overlapping of dehydration and decarbonation

Table 1 Chemical composition of CAC, SF and FA (mass%)

	LI	IR	SiO_2	Al_2O_3	Fe_2O_3	CaO (total)	MgO	SO_3	Na_2O	K_2O	CaO (free)
CAC	0.42	2.24	2.52	43.86	14.2	35.7	0.69	–	0.15	0.1	0.11
SF	0.09	0.06	92.7	0.60	3.78	1.31	0.93	–	0.15	0.37	0.01
FA	2.24	0.53	54.3	26.9	5.38	4.52	2.24	–	0.61	3.17	0.15

LI: lost on ignition; IR: insoluble residue

Table 2 Mass loss/% of solid phases in mixes after 2, 7, 30 and 90 days

Sample	REF				20SF				30SF			
Days	2	7	30	90	2	7	30	90	2	7	30	90
$Al_2O_3{\cdot}xH_2O$ (353–393 K) [16, 24]	1.0± 0.004	0.5± 0.002	1.2± 0.005	0.4± 0.002	1.87± 0.007	1.99± 0.008	3.19± 0.012	0.71± 0.003	1.96± 0.008	1.99± 0.008	2.64± 0.010	1.24± 0.005
CAH_{10}–C_2AH_8 (393–473 K) [16, 25–27]	1.19± 0.005	0.98± 0.004	0.96± 0.004	0.70± 0.003	4.94± 0.019	5.59± 0.022	5.2± 0.020	1.69± 0.007	4.78± 0.019	5.59± 0.022	4.66± 0.019	2.18± 0.009
AH_3 (493–553 K) [16, 24, 25]	6.67± 0.027	7.09± 0.028	9.18± 0.037	7.73± 0.031	5.19± 0.020	5.43± 0.022	5.15± 0.021	5.16± 0.021	4.79± 0.019	5.43± 0.022	4.84± 0.019	4.53± 0.018
C_3AH_6 or $C_3AS_{3-X}H_{2X}$ (553–623 K) [16, 25, 27]	8.01± 0.032	6.99± 0.028	3.91± 0.016	5.28± 0.021	1.01± 0.004	0.84± 0.003	0.85± 0.003	5.99± 0.024	0.92± 0.004	0.84± 0.003	1.29± 0.005	5.72± 0.023
Carbonates (933–998 K) [13]	0.32± 0.001	1.29± 0.002	4.40± 0.009	6.39± 0.013	0.48± 0.001	0.97± 0.002	2.1± 0.004	1.6± 0.003	0.49± 0.001	0.97± 0.002	1.96± 0.004	1.22± 0.002
	50SF				30FA				50FA			
	2	7	30	90	2	7	30	90	2	7	30	90
$Al_2O_3{\cdot}xH_2O$ (353–393 K) [16, 24]	2.28± 0.009	1.89± 0.007	2.28± 0.009	1.12± 0.004	2.19± 0.009	1.35± 0.005	1.75± 0.007	0.48± 0.002	2.36± 0.009	1.70± 0.007	1.94± 0.008	1.06± 0.004
CAH_{10}–C_2AH_8 (393–473 K) [16, 25–27]	4.77± 0.019	4.69± 0.019	4.94± 0.020	2.55± 0.010	4.99± 0.020	5.29± 0.021	4.79± 0.019	1.12± 0.004	5.25± 0.021	4.82± 0.019	4.50± 0.018	1.98± 0.008
AH_3 (493–553 K) [16, 24, 25]	3.26± 0.013	3.08± 0.012	2.96± 0.012	3.69± 0.015	6.20± 0.025	6.72± 0.027	5.56± 0.022	5.23± 0.021	3.24± 0.021	3.73± 0.015	3.16± 0.013	3.96± 0.016
C_3AH_6 or $C_3AS_{3-X}H_{2X}$ (553–623 K) [16, 25, 27]	0.61± 0.002	0.53± 0.002	0.63± 0.002	0.72± 0.003	1.60± 0.006	1.13± 0.004	1.41± 0.006	6.62± 0.026	0.91± 0.004	0.84± 0.003	0.85± 0.003	5.36± 0.021
Carbonates (933–998 K) [13]	0.32± 0.001	0.7± 0.001	0.62± 0.001	2.79± 0.006	0.19± 0.001	0.69± 0.001	2.44± 0.005	1.05± 0.002	0.16± 0.001	0.53± 0.001	2.31± 0.005	1.19± 0.002

processes of different solid phases; however an estimation of the mineral content, based on the mass loss, can be made in some cases. Calculations of mass loss from TG curves, for some solid phases are presented in Table 2. Figure 1 shows the differential thermal analysis, DTA curves, for all the formulations, at 2, 7 and 30 hydration times.

The major endothermic effects recorded afterwards can be attributed to dehydration of $Al_2O_3{\cdot}xH_2O$, CAH_{10}, C_2AH_8, AH_3 and carbonates. The initial step in the thermal decomposition of samples is the endothermic effect at ~360 K, which is induced by $Al_2O_3{\cdot}xH_2O$ (Fig. 1). The loss of mass related with this endothermic effect increases with the introduction of mineral addition in the paste formulation (Table 2), indicating that an amorphous aluminium hydroxide is produced as a product formed in the hydration reaction of calcium aluminates and silica fume or fly ash. However, the broadening of endotherms at the temperature range from 333–393 K in samples including mineral additions indicates the presence of a higher amount of

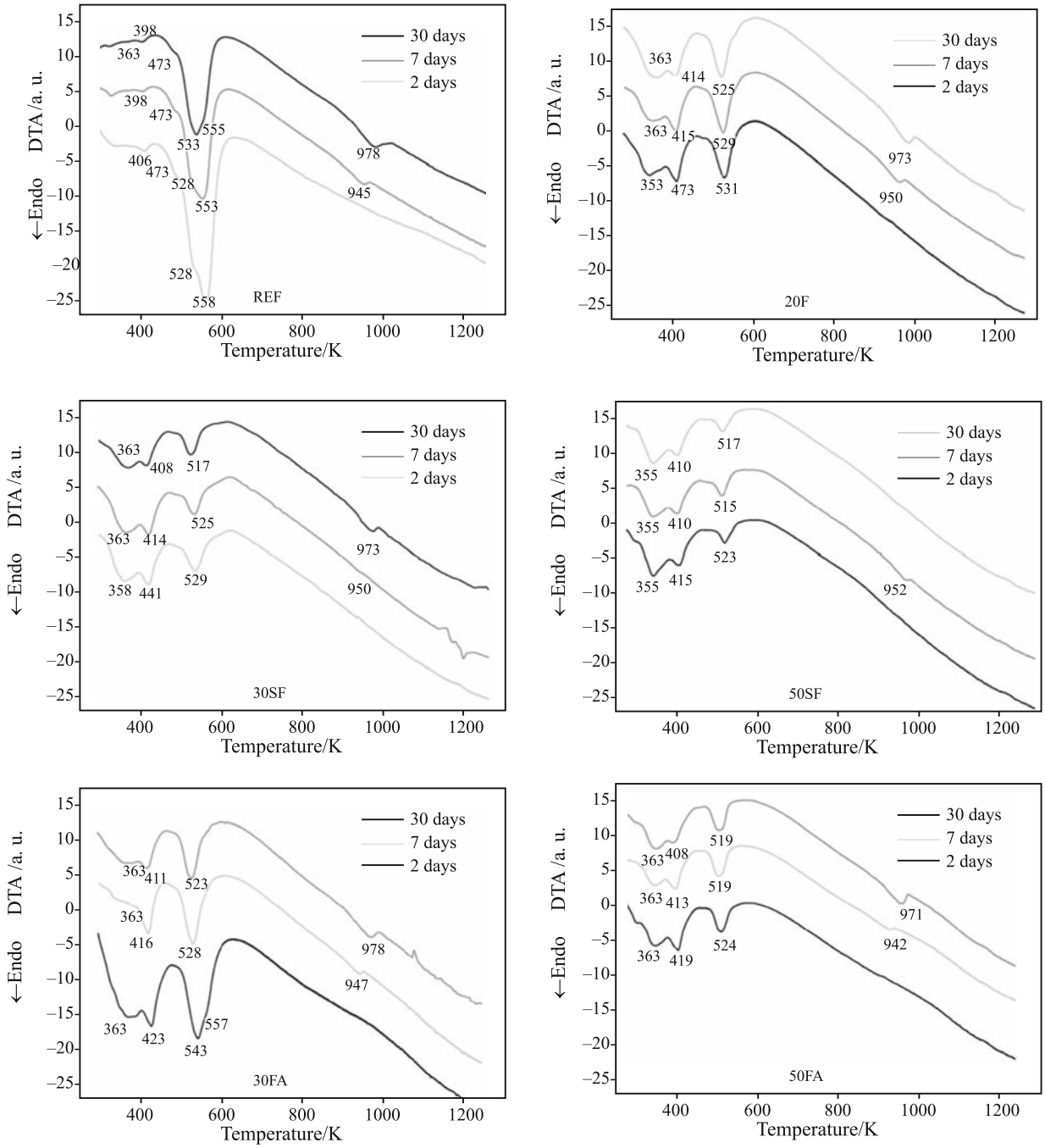

Fig. 1 DTA curves of cement pastes at 2, 7 and 30 days of hydration

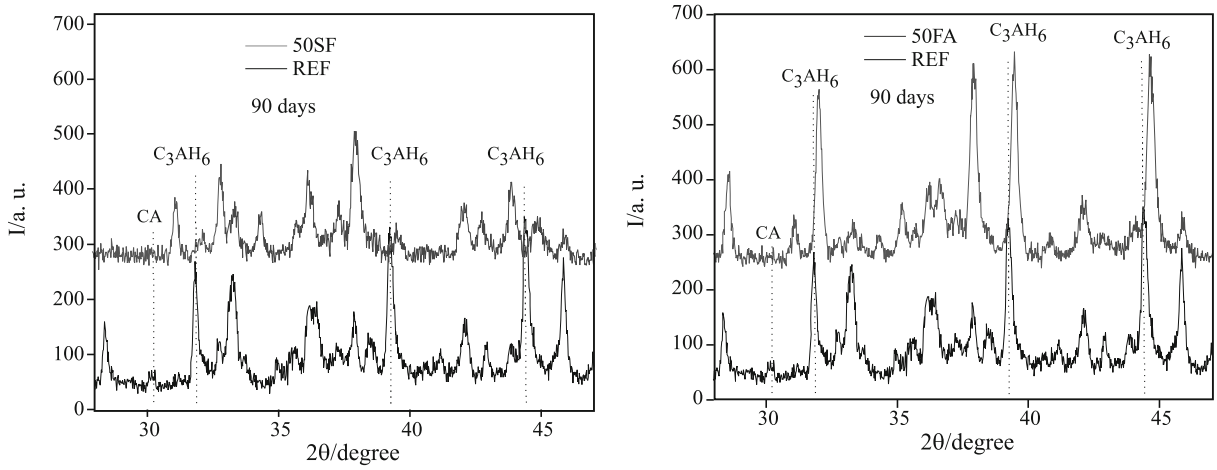

Fig. 2 X-ray powder diffraction of REF, 50SF and 50FA at 90 days hydration

Table 3 Mineralogical composition of the fabricated pastes at the different reaction times

	Days											
	2	7	30	90	2	7	30	90	2	7	30	90
Sample	REF				20SF				30SF			
CA	x	x	x	x	xxx	xx	xx	x	xx	xx	x	x
CAH_{10}	x	–	–	–	xx	xx	–	–	xxx	x	–	–
C_2AH_8	x	–	–	–	xx	xx	–	–	xx	xx	–	–
$C3AS_{3-X}H_{2X}$	x	xxx	xxx	xxx	–	x	xxx	xxx	–	x	xxx	xxx
$C_{12}A_7$	xxx	xxx	xxx	xxx	x	x	x	x	x	x	x	x
C_4AF	x	x	x	x	x	x	x	–	x	x	–	–
AH_3	x	xx	xxx	xxx	x	xx	xx	xx	x	xx	xx	xx
C_2ASH_8	–	–	–	–	–	x	x	x	–	x	xx	xx
CAS_4H_4	–	–	–	–	–	–	x	x	–	–	x	x
C_3AS_3	–	–	–	–	–	–	x	x	–	x	x	x
C_4AcH_{11}	–	–	–	–	x	x	x	–	x	x	x	–
Aragonite	x	x	x	x	x	x	x	x	x	x	x	x
Calcite	x	x	x	x	x	x	x	x	x	x	x	x
Sample	50SF				30FA				50FA			
Days	2	7	30	90	2	7	30	90	2	7	30	90
CA	xx	xx	x	x	xxx	xx	xx	x	xx	xx	x	x
CAH_{10}	xx	x	–	–	xx	xx	–	–	xxx	x	–	–
C_2AH_8	xx	x	–	–	xx	xx	–	–	xx	xx	–	–
$C_3AS_{3-X}H_{2X}$	–	x	xxx	xxx	–	x	xxx	xxx	–	x	xxx	xxx
$C_{12}A_7$	x	x	x	x	x	x	x	x	x	x	x	x
C_4AF	x	x	–	–	x	x	x	x	x	x	–	–
AH_3	x	x	x	x	x	xx	xx	xx	x	xx	xx	xx
C_2ASH_8	x	xx	xxx	xxx	–	x	x	x	–	x	xx	xx
CAS_4H_4	–	x	xx	xx	–	–	–	–	–	–	x	x
C_3AS_3	–	x	xx	xx	–	–	–	–	–	x	x	x
C_4AcH_{11}	x	x	x	–	x	x	x	–	x	x	x	–
Aragonite	x	x	x	x	x	x	x	x	x	x	x	x
Calcite	x	x	x	x	x	x	x	x	x	x	x	x

x: <10 mass%; xx: 10–20 mass%; xxx: >20 mass%. C_3AH_6 is one of the end members of the solid solution $C_3AS_{3-X}H_{2X}$

Table 4 Shift of the measured diffraction peaks with respect to the powder diffraction file: 24-0217 (ICDD 2000 and ICSD data base)

Sample	2θ/degree (measured)	2θ/degree C_3AH_6 Pattern (27-0217)	Difference	2θ/degree CA Pattern (34-0440)	Difference
REF	17.28	17.28 (I_{rel}=90)	0.01		
	19.96	19.97 (I_{rel}=40)	0.01		
	26.52	26.52 (I_{rel}=55)	0		
	28.36	28.4 (I_{rel}=45)	0.04		
	30.08			30.08 (I_{rel}=100)	0
	31.82	31.82 (I_{rel}=80)	0		
	35.66			35.62 (I_{rel}=35)	0.04
	39.22	39.22 (I_{rel}=100)	0		
	44.36	44.39 (I_{rel}=95)	0.03		
	52.48	52.43 (I_{rel}=40)	0.05		
20SF	17.32	17.27 (I_{rel}=90)	0.05		
	20.04	19.97 (I_{rel}=40)	0.07		
	26.62	26.52 (I_{rel}=55)	0.1		
	28.46	28.4 (I_{rel}=45)	0.06		
	30.08			30.08 (I_{rel}=100)	0
	31.94	31.82 (I_{rel}=80)	0.12		
	35.62			35.62 (I_{rel}=35)	0
	39.42	39.22 (I_{rel}=100)	0.2		
	44.52	44.39 (I_{rel}=95)	0.13		
	52.64	52.43 (I_{rel}=40)	0.21		
30SF	17.34	17.27 (I_{rel}=90)	0.07		
	20.08	19.97 (I_{rel}=40)	0.11		
	26.62	26.52 (I_{rel}=55)	0.1		
	28.48	28.4 (I_{rel}=45)	0.08		
	30.08			30.08 (I_{rel}=100)	0
	31.94	31.82 (I_{rel}=80)	0.12		
	35.66			35.62 (I_{rel}=35)	0.04
	39.38	39.22 (I_{rel}=100)	0.16		
	44.52	44.39 (I_{rel}=95)	0.13		
	52.64	52.43 (I_{rel}=40)	0.21		
50SF	17.42	17.27 (I_{rel}=90)	0.15		
	20.24	19.97 (I_{rel}=40)	0.27		
	26.66	26.52 (I_{rel}=55)	0.14		
	28.64	28.40 (I_{rel}=45)	0.24		
	30.08			30.08 (I_{rel}=100)	0
	32.16	31.82 (I_{rel}=80)	0.34		
	35.68			35.62 (I_{rel}=35)	0.06
	39.48	39.22 (I_{rel}=100)	0.26		
	43.96	44.39 (I_{rel}=95)	0.43		
	52.68	52.43 (I_{rel}=40)	0.25		

Table 4 Continued

Sample	2θ/degree (measured)	2θ/degree C3AH6 Pattern (27-0217)	Difference	2θ/degree CA Pattern (34-0440)	Difference
30FA	17.40	17.27 (Irel=90)	0.13		
	20.12	19.97 (Irel=40)	0.15		
	26.66	26.52 (Irel=55)	0.14		
	28.64	28.4 (Irel=45)	0.24		
	30.06			30.08 (Irel=100)	0.02
	32	31.82 (Irel=80)	0.18		
	35.62			35.62 (Irel=35)	0
	39.50	39.22 (Irel=100)	0.28		
	44.64	44.39 (Irel=95)	0.25		
	52.74	52.43 (Irel=40)	0.31		
50FA	17.27	17.27 (I_{rel}=90)	0.11		
	20.12	19.97 (I_{rel}=40)	0.15		
	26.68	26.52 (I_{rel}=55)	0.14		
	28.6	28.4 (I_{rel}=45)	0.20		
	30.06			30.08 (I_{rel}=100)	0.02
	32.02	31.82 (I_{rel}=80)	0.20		
	35.60			35.62 (I_{rel}=35)	0.02
	39.46	39.22 (I_{rel}=100)	0.24		
	44.60	44.39 (I_{rel}=95)	0.21		
	52.7	52.43 (I_{rel}=40)	0.27		

combined water associated with increased quantity of alumina gel and other hydrated minerals.

The endotherm around 410 K is attributed to the dehydration of hexagonal calcium aluminate hydrates, i.e. CAH_{10} and C_2AH_8. The content of hexagonal hydrates is higher for formulations including silica fume or fly ash on their composition, as can be seen in Table 2 and Fig. 1, fact that can be related with the deceleration of the conversion reaction. Additionally these samples including FA or SF on their compositions show a decrease on the hexagonal hydrates content with time, while the content of a member of the grossular-hydrogrossular solid reaction ($C_3AS_{3-X}H_{2X}$) increases, as can be observed in Table 2. However, in the paste with a 50% of silica fume, the hexagonal hydrate content (CAH_{10} and C_2AH_8) is higher than the $C_3AS_{3-X}H_{2X}$ one.

Endothermic peaks in the range 553–623 K indicate the presence of a member of the hydrogarnet series, $C_3AS_{3-X}H_{2X}$, with x:0 to 3 (hydrogarnet). The introduction of silica in the structure of hydrogarnet, C_3AH_6 and the decrease in cristallinity degree, could produce a displacement of the endothermic effect and the overlapping with that one of gibbsite. This could be the reason for the presence of one peak centred at 523 K for the samples including mineral addition, instead of the two ones in the range 523–563K as in REF sample.

In all samples gibbsite shows endotherms at 493–553 K. Gibbsite content decreases with the increase on SF or FA content on formulations (Table 2). The decrease in gibbsite content can be related with the elimination of conversion reactions (1) and (2).

In general, carbonates show peaks at the temperature range of 898–1148 K. In the 2 and 7 days hydrated samples, the decarbonation occurred at lower temperature (the peak temperature was ≈940 K). This fact can be related with the presence of different types of carbonates, different content or different crystallinity degree.

X-ray diffraction (XRD)

Table 3 shows the crystalline phases present in the samples object of this study. After 90 days hydration, the main component of pastes is an aluminosilicate member of the solid solution grossular (C_3AS_3)-hydrogrossular (C_3AH_6), represented in general as $C_3AS_{3-x}H_{2x}$. It is well known that an isomorphous replacement in the XRD pattern produces a variation of pattern peaks. Due to the Si introduction, it was observed that all samples displayed some differences in diffraction patterns; that is a shift of measured diffraction peaks of C_3AH_6 theoretical ones

Table 5 Assignments of mid-infrared absorption bands in REF, 50SF and 50FA samples

REF		50SF		50FA	
ν cm^{-1}	Assignment	ν cm^{-1}	Assignment	ν cm^{-1}	Assignment
		3674 (2 and 7 d)*	O–H stretch in C_4AcH_{11}	3676 (2 and 7 d)	O–H stretch in C_4AcH_{11}
3661	O–H stretch in hydrogarnet	3665(30 and 90 d)	O–H stretch in hydrogarnet	3665 (30 and 90 d)	O–H stretch in hydrogarnet
3624	OH stretch in gibbsite	3621	OH stretch in gibbsite	3622	OH stretch in gibbsite
3529	OH stretch in gibbsite	3527	O–H stretch in gibbsite	3525	O–H stretch in gibbsite
3469	OH stretch in gibbsite	3471	O–H stretch in gibbsite	3469	O–H stretch in gibbsite
3380	OH stretch in gibbsite	3370	O–H stretch in gibbsite	3376	O–H stretch in gibbsite
1637	OH bending of water	1639	OH bending of water	1640	OH bending of water
1480	CO_3^{2-} assymmetric stretching in aragonite+vaterite	1481	CO_3^{2-} assymmetric stretching in aragonite+vaterite	1482	CO_3^{2-} assymmetric stretching in aragonite+vaterite
1429	CO_3^{2-} assymmetric stretching in calcite	1418	CO_3^{2-} assymmetric stretching in calcite	1416	CO_3^{2-} assymmetric stretching in calcite
		1366 (2, 7 and 30 d	CO_3^{2-} assymmetric stretching in C_4AcH_{11}	1364 (2 and 7 d)	CO_3^{2-} assymmetric stretching in C_4AcH_{11}
		1120	assymmetric Si–O–Si stretching in silica fume		
1024	OH bending in gibbsite			1016	OH bending in gibbsite
970	OH bending in gibbsite	968 (7, 30 and 90 d)	OH bending in gibbsite	968 (7, 30 and 90 d)	OH bending in gibbsite
913	OH bending in gibbsite	909 (30 and 90 d)	OH bending in gibbsite	907 (30 and 90 d	OH bending in gibbsite
875 (30 and 90 d)	CO_3^{2-} out of plane bending calcite+vaterite	875 (30 and 90 d)	CO_3^{2-} out of plane bending calcite+vaterite	877 (7, 30 and 90 d)	CO_3^{2-} out of plane bending calcite+vaterite
856	CO_3^{2-} bending aragonite	855 (30 and 90 d)	CO_3^{2-} bending aragonite	857 (7, 30 and 90 d)	CO_3^{2-} bending aragonite
797	OH bending in gibbsite	798	OH bending in gibbsite	793 (30 and 90 d)	OH bending in gibbsite
743	CO_3^{2-} bending vaterite	746 (90 d)	CO_3^{2-} bending vaterite	743 (30 and 90 d)	CO_3^{2-} bending vaterite
658	additional vibration in gibbsite	668	additional vibration in gibbsite	666	additional vibration in gibbsite
		576	C_4AcH_{11}	574 (2 and 7 d)	C_4AcH_{11}
555	Al–O vibration in hydrogarnet			556 (7, 30 and 90 d)	Al–O vibration in hydrogarnet

Table 5 Continued

REF		50SF		50FA	
ν cm^{-1}	Assignment	ν cm^{-1}	Assignment	ν cm^{-1}	Assignment
530	additional vibration in gibbsite	534	additional vibration in gibbsite	534	additional vibration in gibbsite
		477	O–Si–O bend. SF		
				455 (30 and 90 d)	additional vibration in gibbsite
		421	C_4AcH_{11}	422	C_4AcH_{11}
408	CAH_{10}				
365	additional vibration in gibbsite	365	additional vibration in gibbsite	365	additional vibration in gibbsite
		306	C_4AcH_{11}	307	C_4AcH_{11}

*2 and 7 d: 2 and 7 days of hydration

(ICDD card 24-0217). The shift of diffraction peaks increases with the introduction of Si in the structure.

Table 4 presents the variation of measured diffraction peaks for each samples, respect to the powder diffraction file 24-0217 (ICDD 2000 and ICSD data base) at 90 days of hydration. The variation respect to remaining anhydrous calcium monoaluminate (CA) peaks (diffraction file 34-0440), is also included. This solid phase could be used as internal standard, because it does not show any variation from its theoretical pattern. The shift can be observed in Fig. 2, which presents the X-ray spectra of REF, 50SF and 50FA samples at 90 days of hydration.

For all samples, the hexagonal phases, CAH_{10} and C_2AH_8, disappear with time so it is possible to suppose that the hexagonal hydrates are transformed into C_3AH_6 for REF sample and the aluminosilicates ($C_3AS_{3-x}H_{2x}$) for mixes with mineral additions.

Gibbsite and aluminosilicates, identified as gehlenite (C_2ASH_8; $Ca_2Al_2SiO_7{\cdot}8H_2O$) and laumontite ($CAS_4H_4$; $CaAl_2Si_4O_{12}{\cdot}4H_2O$), are also identified by XRD. The appearance of grossular (C_3AS_3), an end member of the $C3AS_{3-x}H_{2x}$ solid solution, in samples 20SF, 30SF, 50SF and 50FA, indicates that no more solid solution is formed. Then, the reaction between silica from SF or FA and aluminates, produces the neoformation of aluminosilicates such as laumontite (CAS_4H_4) and gehlenite (C_2ASH_8) (Table 3). The percentage of FA needed to observe the peaks of these phases is higher (50%) than the one needed in mixes with SF (20%). Diffraction peaks corresponding to laumontite and gehlenite appear at different percentages of silica fume (20%) and fly ash (50%).

Carbonates such us aragonite and calcite were also detected in X-ray powder diffraction. Calcium monocarboaluminate hydrate (C_4AcH_{11}) is present at early ages of hydration in the pastes with mineral addition.

Anhydrous phases such as $CaAl_2O_4$ (CA), $Ca_{12}Al_{14}O_{33}$ ($C_{12}A_7$) and brownmillerite, $Ca_2Al_{1.1}Fe^{2+}_{0.9}O_5$ (C_4AF) are still present at advanced ages.

Mid-Infrared Spectroscopy (FTIR)

Table 5 shows the assignments of mid-infrared absorption bands in REF and in those samples with a greater mineral addition content (50SF and 50FA).

Gibbsite or aluminium hydroxide seems to be the main solid phase formed. Bands for gibbsite are identified at 3625, 3525, 3470 and 3380 cm^{-1} in the hydroxyl-stretching region. More gibbsite bands were found at 1025, 970, 915 cm^{-1} and finally low frequency bands at 797, 660 and 365 cm^{-1} [28, 29]. These bands are in the FTMIR spectra of all the samples, but the band at 1025 cm^{-1} can not be detected in the samples with SF due to the overlapping of the 1120 cm^{-1} band. This band corresponds to asymmetric stretching vibrations of Si–O–Si bridging sequences of the silica fume, that indicates that the silica fume is not totally reacted. Samples including mineral additions on their formulations give less resolved bands indicating less cristallyne solid phases. In these cases an alumina gel ($Al_2O_3{\cdot}xH_2O$) is supposed to be formed.

Hydrated calcium monocarboaluminate, $3CaO{\cdot}Al_2O_3{\cdot}CaCO_3{\cdot}11H_2O$ (C_4AcH_{11}) was detected at short hydration times in REF sample. Systems including SF or FA on their formulation show from 7 days of hydration, the transformation of calcium monocarboaluminate hydrate in the $C_3AS_{3-X}H_{2X}$ member. The transformation can be followed by the disappearing of the band at 3760 cm^{-1} and the appearing of a band at 3660 cm^{-1} assigned to the

$C_3AS_{3-X}H_{2X}$ hydrate and the disappearing of the band at 1366 cm^{-1} and the strong increase of the intensity of aragonite main band, 1480 cm^{-1} (Table 5). In such cases, during the transformation of monocarboaluminate, the introduction of silica on the structure can be favoured. In fact, the decomposition of monocarboaluminate hydrate to gehlenite hydrate in the presence of alite (a source of silica), has been described in the literature [30, 31]. Bands in the range 400–500 cm^{-1} are due to deformation of TO_4 tetrahedra (*T*=Si or Al); the increasing in intensity of this band when the mineral addition content increases is consistent with the formation of a polymerized matrix of calcium silicoaluminate hydrates.

The IR spectra of hexagonal hydrates show similarities with each other as might be expected from their common hexagonal plate-type structures [32]; the main difference between cubic hydrates and hexagonal ones is related with the structural formulation $Ca_3[Al(OH)_6]_2$ for cubic hydrogarnet and the disappearance of the H_2O deformational mode located at 1600 cm^{-1}. However, all hydration products can coexist under these conditions and bands are usually overlapped. According to some authors, main bands of $C_3AS_{3-x}H_{2x}$ solid solution hydrates occur at 3660, 900 and 550 cm^{-1} [33]. These bands appear in REF sample from low reaction times (Fig. 2) and from 7 or 28 days hydration in the case of samples including SF or FA on their formulations, fact related with the transformation of calcium monocarboaluminate on a member of the solid solution $C_3AS_{3-x}H_{2x}$.

Conclusions

The effects of the introduction of silica fume or fly ash on calcium aluminate cement pastes and the phase formation were investigated by XRD, DTA-TG and FTIR, with the following results:

- Thermal analyses allow identifying a lower content of gibbsite and a higher content of hexagonal hydrates for samples including mineral addition on their formulations. These facts are related with the deceleration of the called conversion reaction. For a same percentage of mineral addition, the content of hexagonal hydrates is higher in CAC-SF mixes than in CAC-FA ones. This fact is related with the greater silica content of the silica fume.
- The influence of the isomorphous replacement of Al by Si in the hydrogarnet (C_3AH_6) structure is observed in XRD patterns of samples including SF or FA, by the shift of measured diffraction peaks. An increase of mineral addition content causes an increase of Si/Al ratio in aluminosilicates. The appearance of the grossular end member in samples 20SF, 30SF, 50SF and 50FA, induces the neoformation of aluminosilicates such as laumontite and gehlenite.
- The identification of calcium monocarboaluminate in systems CAC+SF and CAC+FA at early ages, has been carried out by infrared spectroscopy. Main bands of $C_3AS_{3-x}H_{2x}$ solid solution hydrates occur at 3660, 900 and 550 cm^{-1}. Modes of comparable intensity and frequency were observed for all samples, but for the studied mixes with mineral additions they appear after 7 days of hydration. This fact was related with the transformation of calcium monocarboaluminate on a member of the solid solution $C_3AS_{3-x}H_{2x}$ and $CaCO_3$.

Acknowledgements

The financial support of ESDRED EC project: 'Engineering Studies and Demonstration of repository Designs', the Spanish waste national management agency 'ENRESA' and Région Poitou-Charentes (Convention 04/RPC-R-120) is greatly acknowledged.

References

1 H. G. Midgley and A. Midgley, Mag. Concr. Res., 27 (1975) 59.
2 A. Capmas and C. M. George, Adv. Cem. Conc. Res, Proc. Eng. Found. Conf., N.H. Durham, Materials Enginering Division, ASCE, (1994) 377.
3 K. Scrivener, J. L. Cabiron and R. Letourneux, Cem. Concr. Res., 29 (1999) 1215.
4 C. H. Fentiman, S. Rashid, J. P. Bayoux, A. Bonin and M. Testud, Calcium Aluminate Cements, Proc. Inter. Symp. at Queen Mary and Westfield College, University of London, 9–11 July, Chapman and Hall, London 1990, p. 272.
5 C. Xiandong and R. J. Kirkpatrick, J. Am. Ceram. Soc., 76 (1993) 409.
6 A. J. Majumdar, B. Singh and R. N. Edmonds, Cem. Concr. Res., 20 (1990) 7.
7 A. J. Majumdar, B. Singh and R. N. Edmonds, Cem. Concr. Res., 20 (1990) 197.
8 K. Quillin, G. Osborne, A. Majumdar and B. Singh, Cem. Concr. Res., 31 (2001) 627.
9 J. Ding, Y. Fu and J. J. Beaudoin, Cem. Concr. Res., 25 (1995) 1311.
10 A. J. Majumdar and B. Singh, Cem. Conc. Res., 22 (1992) 1101.
11 A. J. Majumdar, R. N. Edmonds and B. Singh, Calcium Aluminate Cement, Proc. Inter. Sym. at Queen Mary and Westfield College, University of London, 9–11 July, Chapman and Hall, London 1990, p. 259.
12 M. Collepardi, S. Monosi and P. Piccioli, Cem. Concr. Res., 25 (1995) 961.
13 J. M. Rivas Mercury, X. Turrillas, A. H. de Aza and P. Pena, J. Solid State Chem., 179 (2006) 2988.

14 Y. Fu, J. Ding and J. J. Beaudoin, Proc. 2nd CANMET/ACI Inter. Symp., Las Vegas, USA, June 11–14 1995.
15 S. Bentsen, A. Seltveit and B. Sanderg, Calcium Aluminate Cements, Proc. Inter. Symp. at Queen Mary and Westfield College, University of London, 9–11 July, Chapman and Hall, London 1990, p. 294.
16 J. M. Rivas Mercury, A. H. de Aza, X. Turrillas and P. Pena, Bol. Soc. Esp. Ceram. V., 42 (2003) 361.
17 P. Ubbríaco, P. Bruno, A. Traini and D. Calabrese, J. Therm. Anal. Cal., 66 (2001) 293.
18 J. Lawry, A. Ray, D. Klimesch, P. Thomas, J.-P. Guerbois and J. Harrison, J. Therm. Anal. Cal., 80 (2005) 637.
19 Th. Perraki, G. Kakali and E. Kontori, J. Therm. Anal. Cal., 82 (2005) 109.
20 A. Bakolas, E. Aggelakopoulou, A. Moropoulou and S. Anagnostopoulou, J. Therm. Anal. Cal., 84 (2006) 157.
21 B. Pacewska, G. Blonkowski and I. Wilinska, J. Therm. Anal. Cal., 86 (2006) 179.
22 C. A. Pinto, P. M. Büchler and J. Dweck, J. Therm. Anal. Cal., 87 (2007) 715.
23 H. G. Midgley, J. Therm. Anal. Cal., 13 (1978) 515.
24 R. C. Mackenzie, Differential Thermal Analysis, Academic Press, London and New York 1970.
25 S. K. Das, A. Mitra and P. K. Das Poddar, J. Therm. Anal. Cal., 47 (1996) 765.
26 R. N. Edmonds and A. J. Majumdar, Cem. Concr. Res., 18 (1988) 473.
27 B. Singh, A. J. Majumdar and K. Quillin, Cem. Concr. Res., 29 (1999) 429.
28 R. L. Frost, J. Kloprogge, S. C. Russell and J. L. Szetu, Thermochim. Acta, 329 (1999) 47.
29 J. A. Gadsden, Infrared Spectra of Minerals and Related Inorganic Compounds, Butterworths, London 1975.
30 G. Renaudin, M. Francois and O. Evrard, Cem. Concr. Res., 29 (1999) 63.
31 H. Y. Ghorab, E. A. Kisbar and S. H. Abou Elfetouh, Cem. Concr. Res., 28 (1998) 763.
32 M. A. Trezza and A. E. Lavat, Cem. Concr. Res., 31 (2001) 869.
33 S. Fujita, K. Suzuki, Y. Shibasaki and T. Mori, J. Mater. Cycles Waste Manage, 4 (2002) 70.

Received: March 14, 2007
Accepted: January 3, 2008
Online First: February 4, 2009

DOI: 10.1007/s10973-007-8439-3